SIN integrated optical phased arrays for two-dimensional beam steering at a single near-infrared wavelength

Nicola A. Tyler, Daivid Fowler, Stephane Malhouitre, Stephanie Garcia, Philippe Grosse, Wilfried Rabaud, Bertrand Szelag

Research Article | Vol. 27, No. 4 | 18 Feb 2019 | OPTICS EXPRESS 5851
Optics EXPRESS

SiN integrated optical phased arrays for two-dimensional beam steering at a single near-infrared wavelength

NICOLA A. TYLER, DAIVID FOWLER,* STEPHANE MALHOUITRE, STEPHANIE GARCIA, PHILIPPE GROSSE, WILFRIED RABAUD, AND BERTRAND SZELAG

University Grenoble Alpes and CEA, LETI, Minatec Campus, F-38054 Grenoble Cedex, France
**daivid.fowler@cea.fr*

Abstract: In this work, we present two-dimensional beam steering in the near-infrared using a SiN integrated circuit, containing optical phased arrays. Beam steering was achieved over a range of 17.6° × 3°, at a fixed wavelength of 905 nm. The first dimension was steered via phase differences between the optical phased array channels. The second dimension was accessed by actively switching between various optical phased array sub-devices containing output diffraction gratings with different periods. The characterisation was performed on a wafer-level test station.

1. Introduction

Optical phased arrays (OPAs) have gained significant attention over the past decade due to their potential use in a broad range of advanced technological applications including light detection and ranging (LIDAR), free space communication and holographic displays [1]. This interest arises from the advantage that OPAs enable non-mechanical, arbitrary beam shaping and steering. Furthermore, it has been shown that OPAs can be implemented using integrated photonics, creating a path for low-cost systems with a small physical footprint [2–4]. OPA integration has been explored on various photonic platforms, of which silicon photonics is particularly attractive due to its CMOS compatibility and high refractive index contrast [5]. Advanced OPA circuits have been demonstrated using silicon, such as a fully integrated device for two-dimensional beam scanning [6], ultra-low divergence beams [7,8] and coherent LIDAR circuits [9,10]. However, the use of silicon provides some limitations in terms of wavelength transparency and maximum optical power. Here, silicon nitride (SiN) presents an interesting alternative as outlined in the following.

SiN has recently become of interest for waveguiding in integrated photonics [11,12]. In comparison to silicon, it provides a number of advantages such as more control over its structural properties during the fabrication process and a higher tolerance to process variations due to a lower refractive index contrast (n_{SiN} ~2, n_{SiO2} ~1.5). Furthermore, its transparency window is much larger and is suited for applications at wavelengths down to at least 500 nm. Lastly, weak non-linear losses allow SiN circuits to operate at high optical powers, which is important for time-of-flight LIDAR. SiN has recently been demonstrated for OPA integration [8,13,14].

For LIDAR applications the steering of an optical beam in two dimensions is desirable. Two-dimensional beam steering of integrated OPAs has been achieved using various methods. The first dimension is usually steered by introducing a phase difference between the OPA channels. The second dimension can be steered in the same way, if the array consists of a 2-D matrix [15]. The downside of such a matrix is the difficulty of spacing the individual antennae closely together to ensure a large field of view. For the case of 1-D arrays of grating antennae, steering in the second dimension has be demonstrated using wavelength tuning, which in turn changes the grating emission angle [6]. However, with regards to future, fully-

#346992 https://doi.org/10.1364/OE.27.005851
Journal © 2019 Received 10 Oct 2018; revised 22 Nov 2018; accepted 5 Dec 2018; published 15 Feb 2019

Optics EXPRESS

integrated devices, this method relies on the availability of tunable integrated lasers at a high optical power.

In this work, we present a method for beam steering in two dimensions while retaining the advantages of using 1-D OPAs operating at a single wavelength. We demonstrate an integrated SiN beam-steering circuit with the ability to switch between several OPAs, each able to sweep in a plane with a distinct θ angle, see Fig. 1, and hence enabling steering in two dimensions. Beam steering in a similar fashion, by switching between different devices, has been also recently been suggested using photonic crystal waveguides [16].

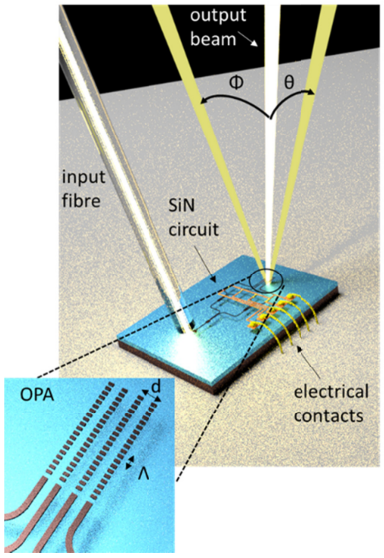

Fig. 1. Artistic illustration of an integrated OPA. The output beam (depicted in white) can be steered in two dimensions (represented in yellow).

2. Design

In this section, the principle behind OPAs will be outlined, followed by the description of our proposed circuit.

2.1 OPA principle

An illustration of an integrated OPA circuit is given in Fig. 1. Light is injected into a single input waveguide, and then split into several channels using Multi-Mode Interference devices (MMIs). Finally, the waveguides recombine to form the OPA output. The OPA output consists of a single diffraction grating per channel, with each channel separated laterally by a certain distance d, where the light is scattered and emitted out of the chip plane. For uniformly spaced channels, the interference pattern of the emitted light in the far field shows maxima that form the fundamental lobe and the higher-order lobes. The fundamental and 1st-order lobes are separated by $\Delta\phi$, which depends on the wavelength λ and the channel distance d

$$\sin \Delta\phi = \frac{\lambda}{d} \tag{1}$$

This distance $\Delta\phi$ defines the useful field of view for LIDAR applications over which the fundamental lobe, hereafter referred to as the *output beam*, can be steered unambiguously. To enable high resolution LIDAR, the divergence of the output beam should be as small as possible. For a given channel spacing, d, the divergence depends on the number of channels. The more channels, the narrower the beam divergence:

Optics EXPRESS

$$\Phi_{3dB} \propto \frac{\lambda}{Nd} \tag{2}$$

where ϕ_{3dB} is the 3 dB beam width and N the number of OPA channels.

In order to describe the emission angle of an OPA, we define two angles, θ and ϕ, which measure the distance of the output beam from the axis orthogonal to the chip plane. θ depends on the grating period Λ, the effective refractive index n_{eff} of the grating, the refractive index of the cladding n_c and the wavelength λ. The emission angle into the cladding θ_c is given by

$$\sin\theta_c = \frac{\Lambda n_{eff} - \lambda}{n_c \Lambda} \tag{3}$$

which is related to the emission angle in air θ according to Snell's law, $\sin\theta = n_c \sin\theta$. The emission angle in the other dimension, ϕ, depends on the linear phase difference ψ between the OPA channels, the wavelength λ and the channel distance d:

$$\sin\phi = \frac{\psi\lambda}{d} \tag{4}$$

Steering the beam in the ϕ dimension can be achieved by introducing a phase shift inside the waveguides before OPA formation, in this case using thermo-optic heaters as illustrated in orange in Fig. 2(a). Steering in the θ dimension however, is more challenging and can be done either by changing the effective refractive index, the grating period or the wavelength, see Eq. (3). In this work, we introduce an approach where a change in grating period is used to achieve beam steering in θ.

Our proposed circuit design for beam steering in two dimensions is shown in Fig. 2(a). In the following, the components which comprise the circuit are described, followed by a description of the circuit functionality.

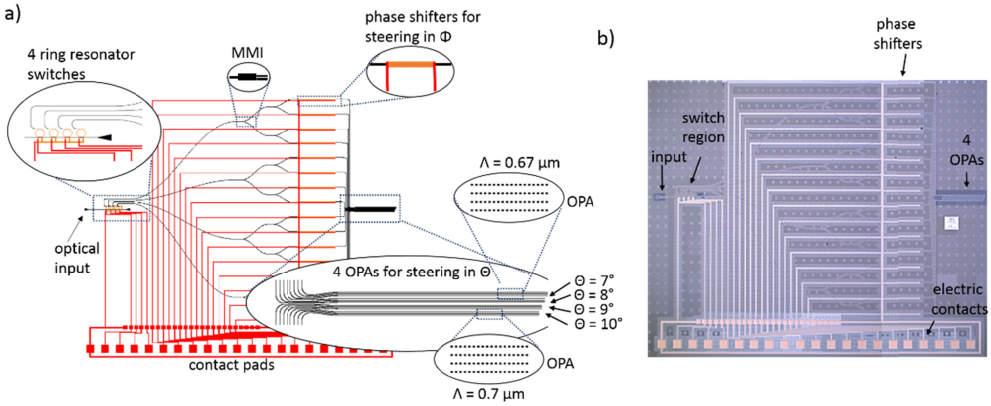

Fig. 2. Schematic and microscope image of the proposed two-dimensional beam steering device. A switching network allows access to four different OPAs, each with distinct emission angle. Phase shifters allow the routing of the light and the introduction of a phase difference between the OPA channels for beam steering.

2.2 Circuit components

In Fig. 2(a), the waveguides are depicted in black, phase shifters in orange and metal contact structures in red. The waveguides are made of Si_3N_4, have a cross section of 300 × 600 nm^2 and are designed to operate in the monomode regime for the TE-polarisation of light at a wavelength of 905 nm. The phase shifters consist of 2 µm-wide and 500 µm-long, resistive Ti/TiN wires. When a voltage is applied to the wires, heat is generated and the SiN refractive

Optics EXPRESS

index is changed due to the thermo-optic effect. This allows a phase shift of the light inside the waveguide. Other components in the circuit include ring resonators and MMIs which are used to route and to split light. Finally, diffraction gratings are used to couple light into the circuit via a fibre grating coupler, and to couple the OPA output to free space. In this case, each OPA contains four output grating couplers, spaced laterally by a distance of 3 μm. In total, the circuit contains four such OPAs, each comprising a different output grating period and designed to emit at θ values between 7° and 10° to the axis orthogonal to the chip plane. The output grating couplers consist of 750 fully etched periods with a nominal filling factor of 0.5 and a variable period between 670 and 700nm. The effective aperture size is related to the grating coupling strength and is simulated to be 90 μm, giving a beam divergence in θ of 0.6°.

2.3 Circuit Operation

After being injected at the input grating coupler, the light reaches a switching network consisting of four ring resonators. By using the phase shifters placed above each ring, light can be routed to the input waveguide of one of the four OPAs. After entering one of these waveguides, the light is then split into four channels at two MMI stages, where phase shifters allow the individual tuning of the phase difference between the channels. Finally, the waveguides recombine at the OPA output. The circuit allows beam steering in the direction of ϕ by adjusting the phase shifters of the OPA channels, and in θ by switching between the OPA devices with differing grating periods. The steering range is limited by an angular range of 17.6° between the 0^{th} and 1^{st} order grating lobes in ϕ, and by the number of available devices in θ, in our case 4°.

3. Fabrication process and performance evaluation

The SiN circuits are fabricated using LETI's 200 mm wafer fabrication platform. A cross-section of the layer structure is given schematically in Fig. 3. A 2.5 μm buffer SiO_2 buffer layer is deposited on a silicon wafer, followed by a 300 nm thick Si_3N_4 layer using low pressure chemical vapour deposition at 750°C. The Si_3N_4 waveguides and gratings were patterned using 248 nm deep ultra violet lithography and plasma dry etching. The waveguides are then encapsulated by 800 nm of planarised SiO_2. A 10 nm / 100 nm patterned Ti / TiN metal layer is used to form heating elements above the waveguides for phase shifting purposes. After further SiO_2 encapsulation and planarisation, vias and metal contact pads are added to electrically connect the heaters.

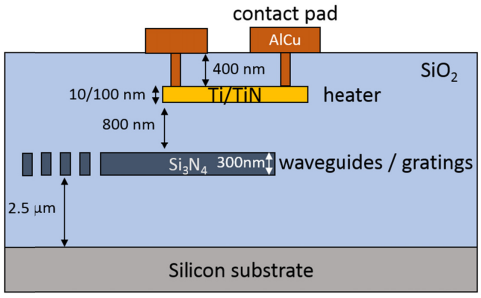

Fig. 3. Schematic of layer structure for SiN integrated circuit for near-infrared wavelengths.

After fabrication, the SiN platform was evaluated in terms of waveguide and coupling losses, as well as phase shifting performance. Cutback measurements yielded a median propagation loss of −1.0 dB/cm. The fibre-grating coupling losses were measured to be - 4.9 dB. This value can be improved in on the future, however different, more efficient, coupling methods are under consideration. The functionality of the phase shifters was evaluated using

Optics EXPRESS

Mach-Zehnder-interferometers. A median electric power of 87.6 mW was measured to lead to a phase shift of π.

4. Characterisation methods

A microscope image of the tested circuit is shown in Fig. 2(b). In order to characterise the far field emission of the OPAs, we have developed a set-up that allows testing at the wafer-scale. A schematic and a picture of the test station are shown in Fig. 4(a) and (b). A 905 nm CW laser is used in conjunction with a polarisation controller as a light source. The alignment of the fibre and the input grating coupler can be optimised with the aid of linear translation stages. For the purpose of imaging the OPA output in the far field, a CMOS sensor (Allied Vision, Prosilica GT 6600) is mounted directly above the wafer at a height of 5 cm. As the beam hits the sensor, the image can be recorded by a computer and analysed. Beam steering can be achieved by controlling the phases of the optical circuit via a 25-channel electric probe.

Voltages are applied to the phase shifters using a custom-made electrical power supply, which can control up to 24 voltages individually. In order to optimise the OPA beam and emit at a desired angle, a computer algorithm was developed. The algorithm tests various different voltages and analyses the resulting output beam recorded by the CMOS sensor. With the use of a hill climbing algorithm, it maximises the ratio of the beam intensity inside a desired output window divided by the intensity outside of that window, while changing the phase shifter voltages.

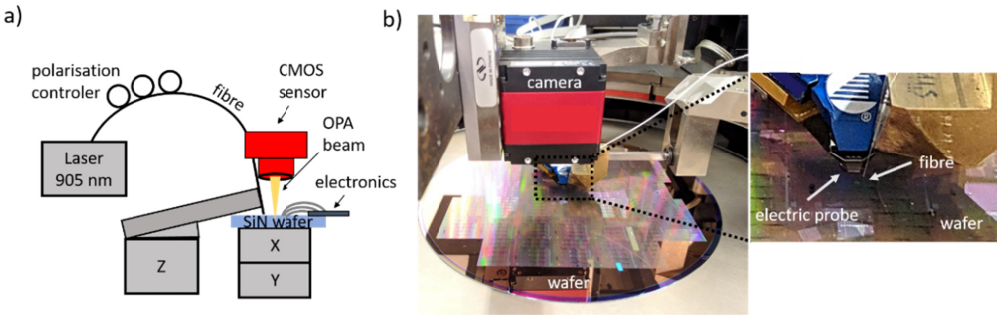

Fig. 4. Schematic and picture of wafer-scale characterisation set-up for OPA measurements. An electronic circuit controls the phase shifter on the optical circuit. The phases can be adjusted and the output beam steered with the feedback of a CMOS sensor imaging the chip output in the far-field.

Finally, in order to relate a recorded intensity spot at the sensor to a certain emission angle, the camera was calibrated. The recorded intensity image of an optimized output beam in the far field is shown in Fig. 5(a) (top image) versus pixel number. A Gaussian curve was fitted across the two maxima corresponding to the 0^{th} and 1^{st} order grating lobes, separated by a known angular separation of 17.6° via the OPA geometry, see Eq. (1). The number of pixels between the two maxima therefore corresponds to a distance of 17.6° and the relationship between pixel and angle was obtained. This process allows relative angles to be obtained, however the absolute emission angles still need to be determined. For this purpose, the output beam was optimised for several angles along ϕ and the intensity of the main lobe recorded. The angle where the main lobe intensity is maximal, around pixel number 2000, was assumed to be the 0° emission point in ϕ. In θ, the absolute angle was determined by fixing the emission of one of the OPA gratings its simulated value of 7°. The final calibrated imaged can be seen in Fig. 5(a) (bottom).

Optics EXPRESS

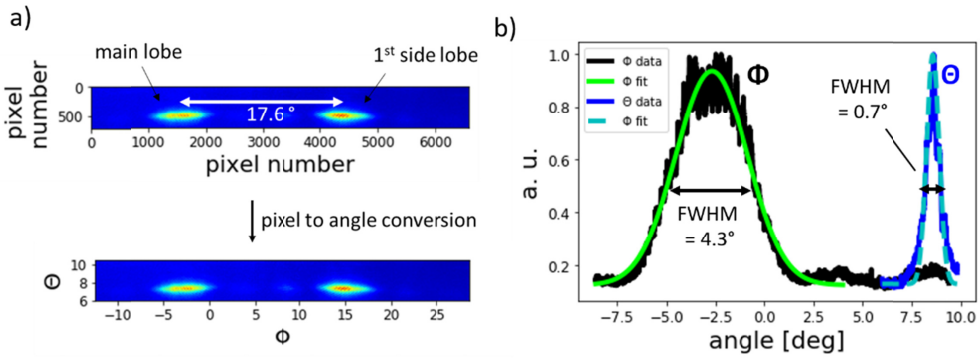

Fig. 5. a) Top: Intensity recorded at the far field camera versus pixel number. The known distance of 17.6° between the two interference maxima was used to obtain a conversion between pixel number and emission angle. The 0° emission is an estimation, as explained in the main text. Bottom: Calibrated intensity image versus ϕ and θ. b) Cross sections in ϕ and θ of the main lobe to determine the FWHM.

5. Beam steering results

The normalised cross sections in ϕ and θ of the main lobe of the optimized beam shown in Fig. 5(a) are given in Fig. 5(b) in black and blue, respectively. A Gaussian curve was fitted to the data in order to obtain the full width at half maximum (FWHM) which corresponds to the 3 dB bandwidth of the beam. The measured FWHM are 4.3° and 0.7° in ϕ and θ. Both values are in in good agreement with the expected beam FWHM in ϕ according to Eq. (2) of 4.3° and the FDTD simulated value of 0.6° in θ.

The beam steering results of the circuit shown in Fig. 2 are given in Fig. 6. Light at a wavelength of 905 nm was used. The OPA output beam was steered in ϕ over the range of 17.6° by adjusting the phases in one of the OPAs. Normalised intensity plots of the beam recorded by the camera versus ϕ and θ at angles of ϕ = - 6°, ϕ = 0° and ϕ = 6° are given in Fig. 6(a) (θ is fixed at 8°). Beam steering over a range of 3° in θ was achieved by routing the input light to various OPAs using the ring switching circuit and optimising the OPA phases to steer to an emission angle of –2° in ϕ. The normalised beam intensities at θ = 7° – 9° are shown in Fig. 6(b) (ϕ is fixed at –2.5°). The light could not be routed to the lowest OPA (for θ = 10°) due to a design error in the switching network. When comparing the beam shapes between the various angles, the shape varies slightly which can be attributed firstly to a non-ideal optimisation routine, and secondly to mechanical oscillations which lead to unstable coupling.

Optics EXPRESS

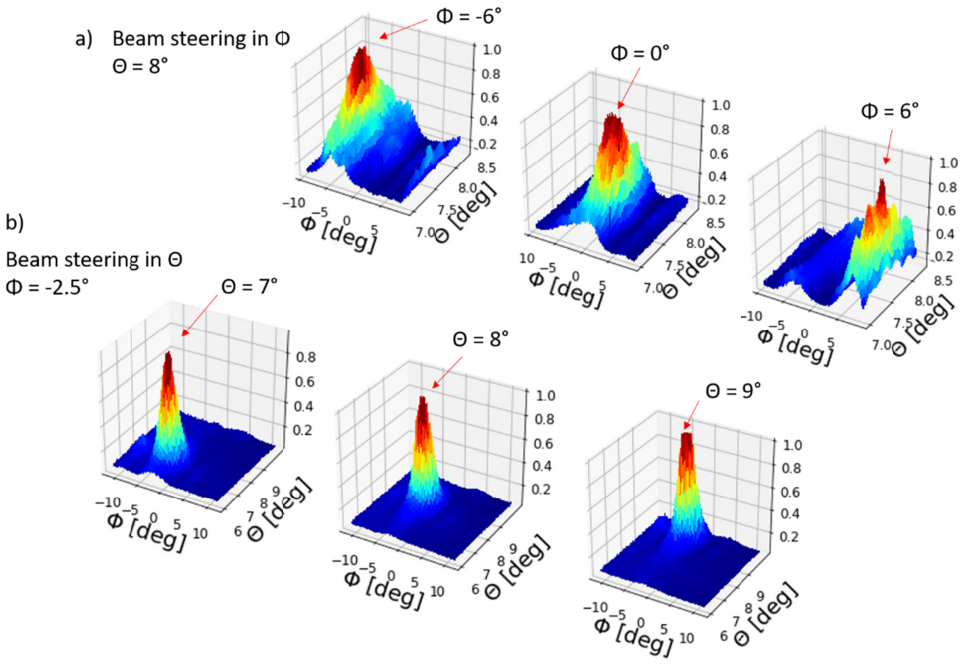

Fig. 6. Beam steering in two dimensions. a) The beam was steered by introducing a phase difference between the OPA channels. b) Bam steering was achieved by switching between three different OPA devices with varying grating periods. Note that the scale in θ varies between the plots in a) and b).

6. Discussion

The above results serve as a proof of principle demonstration, showing that continuous beam steering in ϕ and discrete beam steering in θ is possible using a single integrated device and input wavelength. In the following we will discuss the feasibility of this approach for practical beam scanning applications with a large scanning range and high resolution.

In order to maximise the resolution in θ, the number of OPAs need to be maximised. For practicality, the size of the device should not exceed that of a reticule, which equals a size of 20 mm by 20 mm in our case. In order to optimise the space, the heater cross talk needs to minimised. The effectiveness of 'insulating' waveguide heaters by etching the surrounding cladding material has been previously demonstrated [17]. Our simulations have shown that the efficiency of our SiN waveguide heaters can be increased by up to 10 times when using such methods, and we expect to be able to approach two heaters as close as 2 µm without introducing significant crosstalk.

A 256 channel OPA with 2 µm spacing results in a beam divergence of 0.12° in ϕ, which is sufficiently small for certain practical applications. Assuming a heater spacing of 2 µm, the required height of a 256 channel OPA is 510 µm. Using small bend radii in the MMI tree structure and short heaters, the distance between the first MMI and the end of the OPA can be as small as 2 mm. Such a design results in a footprint of 510 µm × 2 mm = 1.2 mm^2 for a 256 channel OPA. Consequently, tens, or even hundreds, of OPA devices could fit inside a 400 mm^2 reticule together with an appropriate routing network, allowing quasi-continuous scanning over a significant θ range.

7. Conclusion

We have demonstrated a SiN integrated OPA circuit for two-dimensional beam steering. The output beam of the circuit was steered in one dimension by introducing a phase difference

Optics EXPRESS

between the individual OPA channels. The second dimension was accessed by actively routing the input light between several OPA devices containing different grating periods and emission angles. Beam steering was achieved over a range of 17.6° in ϕ and over 3° in θ. The range limitation was given by the higher order grating lobes in ϕ and by the number of devices available on the circuit in θ. More complex circuits based on active routing systems and multiple OPAs may be used to increase the steering range in both dimensions and reduce the beam divergence. The characterisation process was performed on a wafer-level test station. In the future this will allow statistical characterisation of OPA performance on a wafer scale and to select known good devices.

Funding

French Direction Générale des Entreprises (DGE) via the DEMO3S project.

Acknowledgements

The authors would like to thank Olivier Castany for helpful discussions.

References

1. M. J. Heck, "Highly integrated optical phased arrays: photonic integrated circuits for optical beam shaping and beam steering," Nanophotonics **6**(1), 93–107 (2017).
2. F. Vasey, F. K. Reinhart, R. Houdré, and J. M. Stauffer, "Spatial optical beam steerin with an AlGaAs integrated phased array," Appl. Opt. **32**(18), 3220–3232 (1993).
3. K. Van Acoleyen, W. Bogaerts, J. Jágerská, N. Le Thomas, R. Houdré, and R. Baets, "Off-chip beam steering with a one-dimensional optical phased array on silicon-on-insulator," Opt. Lett. **34**(9), 1477–1479 (2009).
4. W. Guo, P. R. Binetti, C. Althouse, M. L. Mašanović, H. P. Ambrosius, L. A. Johansson, and L. A. Coldren, "Two-dimensional optical beam steering with InP-based photonic integrated circuits," IEEE J. Sel. Top. Quantum Electron. **19**(4), 6100212 (2013).
5. B. Jalali and S. Fathpour, "Silicon photonics," J. Lit. Technol. **24**(12), 4600–4615 (2006).
6. J. C. Hulme, J. K. Doylend, M. J. R. Heck, J. D. Peters, M. L. Davenport, J. T. Bovington, L. A. Coldren, and J. E. Bowers, "Fully integrated hybrid silicon two dimensional beam scanner," Opt. Express **23**(5), 5861–5874 (2015).
7. S. Chung, H. Abediasl, and H. Hashemi, "A monolithically integrated large-scale optical phased array in silicon-on-insulator CMOS," IEEE J. Solid-State Circuits **53**(1), 275–296 (2018).
8. C. V. Poulton, M. J. Byrd, M. Raval, Z. Su, N. Li, E. Timurdogan, D. Coolbaugh, D. Vermeulen, and M. R. Watts, "Large-scale silicon nitride nanophotonic phased arrays at infrared and visible wavelengths," Opt. Lett. **42**(1), 21–24 (2017).
9. C. V. Poulton, A. Yaacobi, D. B. Cole, M. J. Byrd, M. Raval, D. Vermeulen, and M. R. Watts, "Coherent solid-state LIDAR with silicon photonic optical phased arrays," Opt. Lett. **42**(20), 4091–4094 (2017).
10. A. Martin, D. Dodane, L. Leviandier, D. Dolfi, A. Naughton, P. O'Brien, T. Spuessens, R. Baets, G. Lepage, P. Verheyen, P. De Heyn, P. Absil, P. Feneyrou, and J. Bourderionnet, "Photonic integrated circuit based FMCW coherent LiDAR," J. Lit. Technol. **36**(19), 4640–4645 (2018).
11. A. Z. Subramanian, P. Neutens, A. Dhakal, R. Jansen, T. Claes, X. Rottenberg, F. Peyskens, S. Selvaraja, P. Helin, B. Du Bois, K. Leyssens, S. Severi, P. Deshpande, R. Baets, and P. Van Dorpe, "Low-Loss Singlemode PECVD Silicon Nitride Photonic Wire Waveguides for 532–900 nm Wavelength Window Fabricated Within a CMOS Pilot Line," IEEE Photonics J. **5**(6), 2202809 (2013).
12. R. Baets, A. Z. Subramanian, S. Clemmen, B. Kuyken, P. Bienstman, N. Le Thomas, G. Roelkens, D. Van Thourhout, P. Helin, and S. Severi, "Silicon Photonics: silicon nitride versus silicon-on-insulator," in Optical Fiber Communication Conference, OSA Technical Digest (online) (Optical Society of America, 2016), paper Th3J.1.
13. S. Sabouri and K. Jamshidi, "Design Considerations of Silicon Nitride Optical Phased Array for Visible Light Communications," IEEE J. Sel. Top. Quantum Electron. **24**(6), 1–7 (2018).
14. M. Zadka, Y.-C. Chang, A. Mohanty, C. T. Phare, S. P. Roberts, and M. Lipson, "On-chip platform for a phased array with minimal beam divergence and wide field-of-view," Opt. Express **26**(3), 2528–2534 (2018).
15. J. Sun, E. Timurdogan, A. Yaacobi, E. S. Hosseini, and M. R. Watts, "Large-scale nanophotonic phased array," Nature **493**(7431), 195–199 (2013).
16. H. Abe, M. Takeuchi, G. Takeuchi, H. Ito, T. Yokokawa, K. Kondo, Y. Furukado, and T. Baba, "Two-dimensional beam-steering device using a doubly periodic Si photonic-crystal waveguide," Opt. Express **26**(8), 9389–9397 (2018).
17. A. Masood, M. Pantouvaki, G. Lepage, P. Verheyen, J. Van Campenhout, P. Absil, D. Van Thourhout, and W. Bogaerts, "Comparison of heater architectures for thermal control of silicon photonic circuits," in Proc. 10th Int. Conf. Group IV Photon., 2013, pp. 83–84.